

## Dielectric Siphons

**Abstract.** *The normally weak polarization force density, exerted on insulating dielectric liquids by a nonuniform electric field, is enhanced if high pressures are used. The result is a new class of orientation and guiding structures for liquids: electric "walls" contain the liquid. The dielectric siphon is an example of such a system. A simple laminar flow model for the device successfully describes the operation of the siphon.*

Insulating dielectric liquids are attracted from regions of lower to regions of higher electric field intensity (even in the absence of free electric charge) through the mechanism of the polarization force. This force can effect fluid orientation in a zero-gravity environment (1, 2). For earthbound experiments in competition with gravity, however, the effect is quite weak because of the relatively low electrical breakdown strength of the dielectric fluid vapors. In an effort to circumvent this

limitation, we have used a high-pressure environment to perform experiments in which the vapor breakdown strength is enhanced, thus allowing the polarization force to dominate. The remote dielectric liquid-handling and orientation capabilities observed are of general interest. Jones has reviewed the classes of electrohydrostatic equilibria associated with the polarization force, using pressures up to 25 atm in order to study these equilibria experimentally (3). The fluid orientation structures

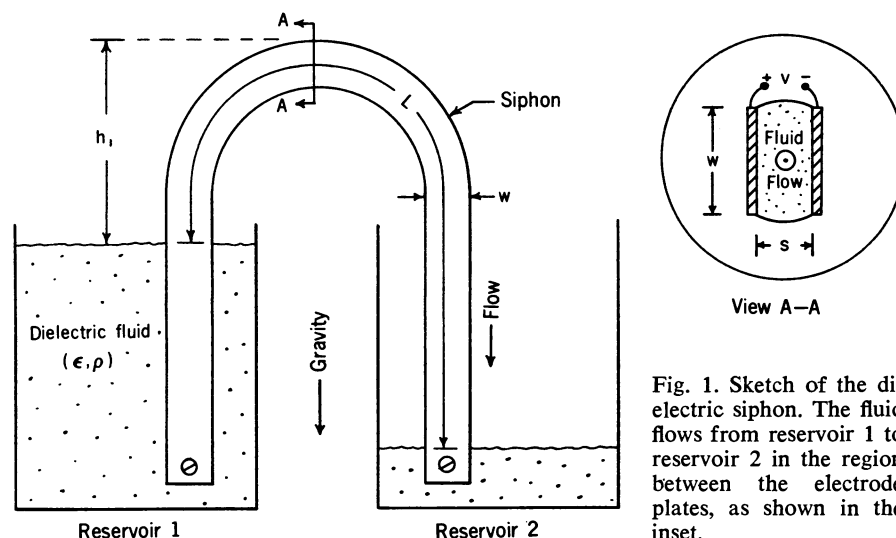


Fig. 1. Sketch of the dielectric siphon. The fluid flows from reservoir 1 to reservoir 2 in the region between the electrode plates, as shown in the inset.

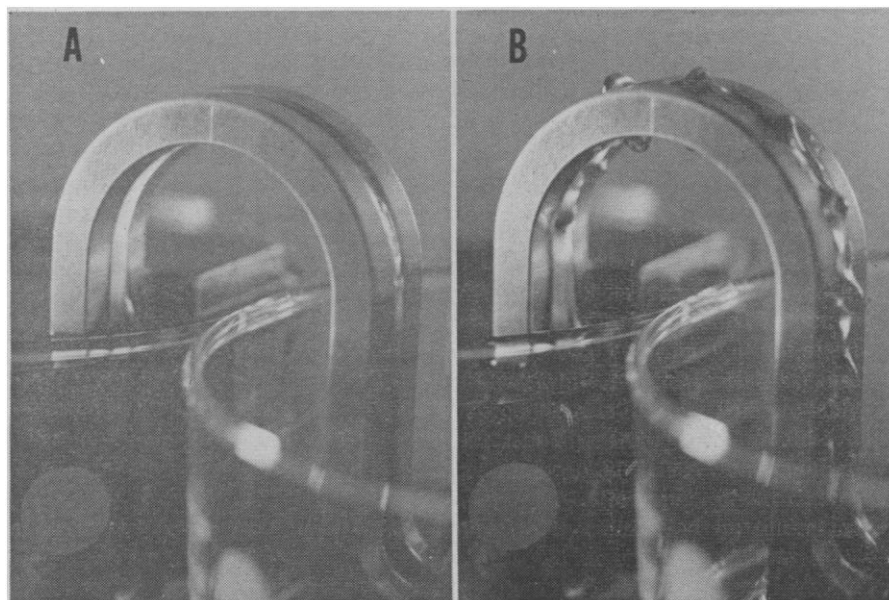


Fig. 2. (A) Photograph of the dielectric siphon, with  $s \approx 0.3$  cm and  $V = 20$  kv (root-mean-square). (B) Photograph of the dielectric siphon, with  $s \approx 0.3$  cm and  $V = 30$  kv (root-mean-square). The surface exhibits parametric instability.

are not limited to static situations; they may be used to guide moving dielectric fluid (2), much as a channel guides water. The nonuniform electric field acts as an elastic "wall" to contain and guide the dielectric fluid. A general theory for these electrohydrodynamic (EHD) conduits has been developed (4) and experimentally verified (5).

An illustrative example of these EHD conduits is the dielectric siphon (Fig. 1), consisting of two U-shaped electrodes held adjacent to each other at a spacing  $s \approx 0.3$  cm by insulating nylon screws. The two legs of the inverted U-shaped structure are dipped into two reservoirs, one filled with dielectric liquid and the other empty. The entire structure is placed inside a pressure vessel, which is then pressurized to several hundred pounds per square inch of dry  $N_2$  gas. Then an alternating voltage [ $>19$  kv (root-mean-square value)] is applied between the electrodes. In order to avoid the accumulation of free surface charge, the frequency of this voltage is made much higher ( $\sim 400$  hz) than the reciprocal charge relaxation time (6), and thus the liquid responds primarily to the time-average electrical stress. The dielectric liquid, as a result of the polarization force, rises against gravity between the electrodes. The height  $h$  to which the fluid rises in such a system is given by (7)

$$h \approx \frac{(\epsilon - \epsilon_0) V^2}{2\rho g s^2} \quad (1)$$

where  $\epsilon$  and  $\rho$  are the dielectric constant and the density of the liquid, respectively,  $V$  is the applied voltage,  $g$  is the acceleration of gravity,  $s$  is the electrode spacing, and  $\epsilon_0$  is the permittivity of free space. If the voltage (Fig. 1) is raised so that  $h \geq h_1$ , dielectric liquid will reach the top of the siphon and gravity will pull it down on the other side. Then the entire inter-electrode region will fill with dielectric fluid.

Once "primed," the dielectric siphon functions much like a conventional siphon (although it will not continue to function if the voltage is removed); the gravitational driving head due to the difference in reservoir levels balances the dynamic viscous head loss, with dielectric liquid flowing so as to equalize these levels. Figure 2, A and B, shows the experiment. In Fig. 2B we have raised the voltage to the point where parametric surface instability sets in (3). The wavy surface helps to indicate the presence of liquid between

the electrodes. There are several important points about the siphon that should be mentioned:

1) The dielectric siphon is self-priming and can be controlled remotely by the voltage  $V$ .

2) Once  $V$  is raised beyond the threshold, the fluid cross section remains essentially constant, and so the flow rate of the parallel-plate device (Fig. 1) is independent of voltage. (Other dielectric siphons are envisioned, in which continuous flow control would be achieved.)

3) The electrical polarization force present does *not* pump the dielectric liquid, but merely provides an orientation configuration with fluid communication between the two reservoirs. As with any true siphon, gravity does the pumping.

To test the theoretical model for the dielectric siphon, Perry measured indirectly the flow rate as a function of time for various siphon parameters (8). If we assume viscous laminar (Poiseuille) flow between the electrode plates and neglect inlet and outlet flow losses, the theoretical rate of volume flow  $Q$  in the siphon is a decaying exponential function of time  $t$  with a time constant  $\tau^*$ :

$$Q(t) = Q_0 e^{-t/\tau^*} \quad (2)$$

$$\tau^* = \left( \frac{A_1 A_2}{A_1 + A_2} \right) \frac{12 \mu L}{g S^2 w \rho}, \quad A_1 \simeq A_2 \quad (3)$$

where  $Q_0$  is the theoretical rate of volume flow at time  $t=0$ ,  $A_1$  and  $A_2$  are the cross-sectional areas of the two reservoirs,  $\mu$  is the dynamic liquid viscosity,  $L$  is the working length of the siphon, and  $w$  is the electrode width (for the experiment reported  $h$  was approximately 2.5 to 5 cm). Plots of the experimental values of  $Q$  versus  $t$

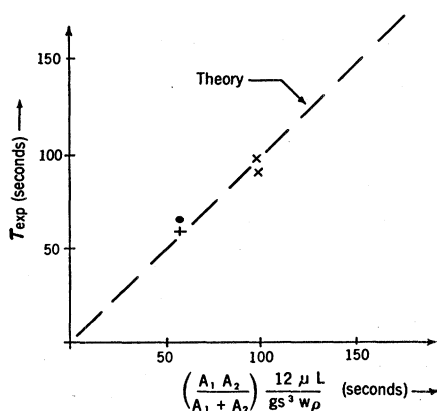


Fig. 3. Plot of the experimental time constant  $\tau_{\text{exp}}$  versus the theoretical time constant  $\tau^*$ . Root-mean-square voltages are as follows:  $\times$ , 19 kv;  $\bullet$ , 30 kv;  $+$ , 34 kv.

on semilogarithmic paper are linear, an indication of the validity of Eq. 2. Figure 3 shows a plot of the time constants taken from numerous experimental measurements, with a theoretical curve from Eq. 3. The results are independent of the influence of the applied voltage  $V$ .

THOMAS B. JONES

Department of Electrical Engineering,  
Colorado State University,  
Fort Collins 80521

MICHAEL P. PERRY

Inforex, Inc.,  
Burlington, Massachusetts 01803

JAMES R. MELCHER

Department of Electrical Engineering,  
Massachusetts Institute of Technology,  
Cambridge 02139

#### References and Notes

1. J. R. Melcher, D. S. Guttman, M. Hurwitz, *J. Spacecr. Rockets* **6**, 25 (1969).
2. J. R. Melcher, M. Hurwitz, R. G. Fax, *ibid.*, p. 961.
3. T. B. Jones, thesis, Massachusetts Institute of Technology (1970).
4. ——— and J. R. Melcher, in preparation.
5. T. B. Jones, in preparation.
6. E. B. Devitt and J. R. Melcher, *Phys. Fluids* **8**, 1193 (1965).
7. H. Pellat, *C. R. Seances Acad. Sci. Paris* **119**, 675 (1894).
8. M. P. Perry, thesis, Massachusetts Institute of Technology (1969).
9. The work reported here was performed at the Massachusetts Institute of Technology, Cambridge. This work is based in part on a thesis entitled "Dielectrophoretic siphons" submitted (by M.P.P.) to the Department of Electrical Engineering at the Massachusetts Institute of Technology in partial fulfillment of the requirements for the degree of Bachelor of Science. We thank Prof. J. G. Trump of the High Voltage Research Laboratory for the loan of a pressure vessel. Supported by NASA grant NGL-22-009-014.

13 August 1971

## Nuclear Acidic Protein Changes during Differentiation in *Physarum polycephalum*

**Abstract.** A class of acidic nuclear phosphoproteins has been isolated throughout the mitotic cycle and at two points during differentiation in the slime mold *Physarum polycephalum*. The electrophoretic profiles of these proteins are reproducible and unchanging throughout the mitotic cycle, but reproducible changes occur during differentiation. The proteins are rapidly synthesized after mitosis, and their molecular weights range from 34,000 to 88,000. The proteins rapidly incorporate [ $^{32}\text{P}$ ]orthophosphate, and the content of alkali-labile phosphate increases 20 percent during the period after DNA synthesis. The proteins comprise 6.5 percent by dry weight of nuclear material while the DNA comprises about 5.5 percent. These acidic nuclear proteins may have a role in control of gene activity.

The regular distribution of nuclear histones throughout many types of cells (1, 2), together with the unchanging nature of histones during tissue differentiation (3) and the apparently non-specific nature of histone inhibition of DNA-directed RNA synthesis (4), complicates any model attempting to explain the mechanism of nuclear histones in controlling specific gene expression. In contrast the heterogeneity (5, 6) and tissue specificity (6) of certain acidic nuclear proteins suggests that these acidic proteins may in fact possess the required specificity and variety of types necessary for control of gene activity. Whereas the studies of others (4-11) imply a gene regulatory function for the acidic nuclear proteins, more direct evidence, such as major changes in the electrophoretic profiles of these proteins in differentiating tissue, has not been reported.

This report is concerned with the characterization of a specific phenol-soluble fraction of acidic nuclear proteins in *Physarum polycephalum*. The

procedure for protein isolation was adapted from Teng *et al.* (6). Proteins isolated from nuclei through phenol solubilization have been shown to be synthesized specifically in response to hormones (7), and these proteins are heterogeneous in different tis-

Table 1. Amino acid analysis of PSANP fraction of *P. polycephalum*. The values are the average of three analyses on proteins isolated 4 hours after metaphase III (12).

Amino acid	Content (moles per 100 moles of total amino acid)
Lysine	7.65
Histidine	2.82
Arginine	5.92
Aspartic acid	10.51
Threonine	5.59
Serine	6.95
Glutamic acid	11.53
Proline	5.19
Glycine	8.60
Alanine	8.27
Valine	6.36
Methionine	1.42
Isoleucine	4.86
Leucine	8.34
Tyrosine	2.65
Phenylalanine	3.46